

Analytical solutions of the geodesic equation in the space-time of a black hole surrounded by perfect fluid in Rastall theory

Saheb Soroushfar^{1*} and Maryam Afrooz¹

¹*Faculty of Technology and Mining,*

Yasouj University,

Choram 75761-59836, Iran

(Dated: June 27, 2019)

Abstract

In this paper, we investigate the geodesic motion of massive and massless test particles in the vicinity of a black hole space-time surrounded by perfect fluid (quintessence, dust, radiation, cosmological constant and phantom) in Rastall theory. We obtain the full set of analytical solutions of the geodesic equation of motion in the space-time of this black hole. For all cases of perfect fluid, we consider some different values of Rastall coupling constant $k\lambda$ so that the equations of motion have integer powers of \tilde{r} and also can be solved analytically. These analytical solutions are presented in the form of elliptic and also hyperelliptic functions. In addition, using obtained analytical solution and also figures of effective potential and $L - E^2$ diagrams, we plot some examples of possible orbits. moreover we use of the angular momentum, conserved energy, electrical charge and also Rastall parameter, to classify the different types of the possible gained orbits. Moreover, we show that when Rastall field structure constant becomes zero ($N = 0$) our results are consistent with the analysis of a Reissner-Nordström black hole, however when both Rastall geometric parameter and electric charge vanish ($N = Q = 0$), the metric and results are same as analysis of a Schwarzschild black hole.

*Electronic address: soroush@yu.ac.ir

1. INTRODUCTION

Einstein general relativity (GR) is a geometric gravitational theory which define all solar system observations, the dynamic cosmos and gravitation as a geometrical curvature, which affects the motion of light ray and test particles in space-time [1]. The existence of black hole is one of the important issues in physics which predicted by the equations of GR [2]. Black holes and the metrics that explain the space-time around them are very important fields of study and research, because of having a gravitational influence on their surrounding, and also on motion of light ray and test particles [3], information about the last step of the star life, and discussion of the dark matter. Researchers have posited that the Universe contains dark matter [4, 5] and dark energy [6, 7] which are two important problems of the standard present cosmological model which can explain the accelerating expansion of the cosmos [6]. Dark matter is a scalar field (25 percent of energy content in the Universe) composed of weakly interacting massive particles that interact through weak force whereas dark energy (70 percent of energy content in the Universe) [8] known as an exotic fluid and a type of dynamical quantum vacuum energy or a kind of self-repulsive mysterious force with negative pressure [8–10]. Observational evidence such as Cosmic Microwave Background radiation [11], the large-scale structure of the Universe [12] and luminosity distance of Supernova Type Ia [6, 13] will be known as accelerating expansion phase reasons. Dark energy was proposed to interpret the accelerating rate [1] by a very small positive cosmological constant with a state parameter $\omega = -1$ [9, 10, 14–17]. Recent observations enable the existence of cosmological model including dark energy with an equation of state $\omega < -1$. Quintessence as a candidate for dark energy with state parameters in the range of $-1 < \omega_q < -\frac{1}{3}$ [15, 18], and phantom field with $\omega = -\frac{4}{3}$, are two exotic matters which try to explain the nature of dark energy [9, 18]. A black hole might be surrounded by regular matter like radiation with $\omega = \frac{1}{3}$ and dust with state parameter $\omega = 0$ or exotic matter like cosmological constant, quintessence and phantom fields or combination of them [19].

One of the important results obtained from Einstein fields equations is a null divergence of the energy-momentum tensor in the form $T^{\mu\nu}{}_{;\nu} = 0$ [19]. Due to the violation of the usual classical conservation laws and verification of the condition $T^{\mu\nu}{}_{;\nu} \neq 0$ by particle creation in cosmology [20], a new formulation of the energy-momentum tensor has suggested by quantities related to the curvature of the space-time [21]. In 1972 P. Rastall [22] proposed

a modified theory of general relativity with the new a formulation of connection between energy-momentum tensor, $T^{\mu\nu}$, to the derivative of Ricci scalar, i.e. $T^{\mu\nu}_{;\nu} \propto R^{,\nu}$ [19], which get back to the Einstien's basic assumptions in the empty Universe [23] and represents to the Mach principle [24]. Rastall assumed in curved space-time the usual conservation laws used in GR are collapsed [25]. In other words, for a non-minimal way that the matter and geometry fields are joined together, $T^{\mu\nu}_{;\nu} = \lambda R^{,\nu}$ where λ called the Rastall free parameter which describes the deviation from the Einstein theory of GR and defined from observations [22, 26]. For the universe expansion, Rastall theory can be regenerate some loop quantum cosmological features [26–31] and also has agreement with the cosmic accelerating expansion [32]. Moreover, the effects of quantum fields in curved space-time in a covariant approach can be studied in this theory [19, 33–35]. Due to the correlation of Rastall's theory with the high curvature environments and also, for having more information about the nature of a non-minimal coupling between matter fields and geometry in the Rastall hypothesis, Studding the physical quantities and properties of black holes in Rastall gravity in more details and comparing results with general relativity, can be useful [19]. Therefore, in this paper, our aim is to study the geodesic motion in the space-time of a black hole in Rastall theory.

Since only light and particles are detectable, studying their orbits in space-time near a black hole, is an important tool for investigating physical properties and the features of solutions of Einstein field equations and also for tests of GR. The coupled geodesic equations will describe the motion of system by differential equations based on the metric of the considered field. The equations will be decoupled by evident symmetries [36]. Analysis of geodesic equation of motion is especially useful for analysing the properties of space-time and predict some observational events such as perihelion shift, light deflection and gravitational time-delay [37]. In 1916, Schwarzschild discovered the first exact solution to Einstein's equations in the case of aspherically symmetric black hole in four-dimensional space-time [38]. All analytical solutions of the geodesic equation in a Schwarzschild (AdS) space-time and gravitational field have been presented by Hagihara in 1931 [39].

Many different space-times in theory of general relativity and also in modified theory, such as four-dimensional Schwarzschild-de Sitter [1, 40], higher dimensional Schwarzschild, Schwarzschild-(anti-)de Sitter, Reissner-Nordström, Reissner-Nordström-(anti-)de Sitter [40–42], Kerr [43], Kerr-de Sitter [44] and black holes in $f(R)$ gravity [45], static and rotating

dilaton black hole [37], (2 + 1)dimensional charged BTZ [3], static cylindrically symmetric conformal gravity [46], the higher-dimensional Myers-Perry space-time [47, 48] and geodesics in the spacetime of a rotating charged black hole [49], have been studied and their geodesic equation solved analytically.

In this paper, we study geodesic equation of motion for test particles in the space-time of a black hole surrounded by five perfect fluids such as quintessence, dust (energy matter), radiation, cosmological constant and phantom fields in Rastall theory. We show our analytical solution here in form of elliptic and also hyperelliptic functions. In Section (2) we give a brief review of a black hole surrounded by perfect fluids in Rastall field equations. In section (3) we investigate the analytical solution of the equations of motion for timelike and null geodesic equations with some possible values of Rastall coupling constant for five surrounding fields in five subsections. In section (4), we use the analysis provided in the previous sections for geodesic equations and their analytical solutions, to plot $\tilde{L} - E^2$ diagrams, effective potential and also to analyse the possible orbit types, their classification and plot some examples of possible orbits. we represent conclude in Section (5).

2. FIELD EQUATIONS IN RASTALL THEORY OF GRAVITY

In this section, we give a brief review of the field equations in the context of the Rastall theory of gravity. For a space-time with Ricci scalar R and an energy momentum source of $T_{\mu\nu}$, considering Rastall hypothesis as

$$T_{;\mu}^{\mu\nu} = \lambda R_{;\nu} \quad , \quad (1)$$

The Rastall fields equations can be written as

$$H_{\mu\nu} = G_{\mu\nu} + k\lambda g_{\mu\nu}R = kT_{\mu\nu}, \quad (2)$$

where λ is the Rastall parameter and k is the Rastall gravitational coupling constant [19]. In the limit of $\lambda \rightarrow 0$ and $k = 8\pi G_N$, this equation reduce to GR field equations. The black hole solution can be obtained by considering the general spherical symmetric space-time metric as

$$ds^2 = -f_s(r)dt^2 + \frac{dr^2}{f_s(r)} + r^2(d\theta^2 + \sin^2\theta d\phi^2), \quad (3)$$

where $f_s(r)$ is a generic metric function which must be specified and the subscript "s" indicates the general surrounding field. Nonvanishing components of the Rastall tensor of Eq. 2, can be obtained using metric 3. After that, as to the nonvanishing components of the Rastall tensor $H_{\mu\nu}$, the total energymomentum tensor supporting this space-time, which should also obey the symmetry properties of the Rastall tensor, should have the following form

$$T^\mu{}_\nu = E^\mu{}_\nu + \tau^\mu{}_\nu, \quad (4)$$

where $T^\mu{}_\nu$ explains the energymomentum tensor of the surrounding field, that by taking the isotropic average over the angles, can be defined as

$$\langle \tau^i{}_j \rangle = \omega_s \rho_s \delta^i{}_j = p_s \delta^i{}_j, \quad (5)$$

in which, ω_s , p_s and ρ_s are the equation of state, the pressure and the energy density parameters, respectively. On the other hand, in Eq. 4, $E^\mu{}_\nu$ is the trace-free Maxwell tensor as [19]

$$E_{\mu\nu} = \frac{2}{k} \left(F_{\mu\alpha} F_\nu{}^\alpha - \frac{1}{4} g_{\mu\nu} F^{\alpha\beta} F_{\alpha\beta} \right), \quad (6)$$

where, $F_{\mu\nu}$ is the antisymmetric Faraday tensor. Taking into account the spherical symmetry existing in the space-time metric (3), consequently by considering the only non-vanishing components of the Faraday tensor $F_{\mu\nu}$, the Maxwell tensor $E^\mu{}_\nu$ and the Rastall tensor $H_{\mu\nu}$, and solving the set of related differential equations, the following general solution for the metric function can be obtained as [19]

$$f_s(r) = 1 - \frac{2M}{r} + \frac{Q^2}{r^2} - \frac{N_s}{r^{\frac{1+3\omega_s-6k\lambda(1+\omega_s)}{1-3k\lambda(1+\omega_s)}}}, \quad (7)$$

which it is depended on the Rastall parameters k and λ , radial coordinate r , mass M , the electric charge of the black hole Q , equation of state parameter ω_s and surrounding field structure parameter N_s [19]. Eqs. (3) and (7) for $k = 8\pi G_N$ and $\lambda = 0$ convert to

$$ds^2 = -\left(1 - \frac{2M}{r} + \frac{Q^2}{r^2} - \frac{N_s}{r^{3\omega_s+1}}\right) dt^2 + \frac{dr^2}{1 - \frac{2M}{r} + \frac{Q^2}{r^2} - \frac{N_s}{r^{3\omega_s+1}}} + r^2 d\Omega^2, \quad (8)$$

which represent the Reissner-Nordström black hole surrounded by a surrounding field in GR [50]. By comparing the metrics (3), (7) with (8), some interesting features with introducing an "effective equation of state" has been studied in detail in [19].

3. GEODESICS

The geodesic differential equation is in general of the form

$$\frac{d^2 x^c}{d\lambda^2} + \Gamma_{ba}^c \frac{dx^a}{d\lambda} \frac{dx^b}{d\lambda} = 0, \quad (9)$$

where Γ_{ba}^c are the Christoffel symbols. By using the normalization condition $g_{\mu\nu} \frac{dx^\mu}{ds} \frac{dx^\nu}{ds} = \epsilon$, (where for massive particles $\epsilon = 1$ and for light $\epsilon = 0$), and two constant of motion energy E and the angular momentum L as

$$E = g_{tt} \frac{dt}{ds} = f_s(r) \frac{dt}{ds}, \quad L = g_{\phi\phi} \frac{d\phi}{ds} = r^2 \frac{d\phi}{ds}, \quad (10)$$

and considering the motion is took place in a equatorial plane, $\theta = \frac{\pi}{2}$ as an initial condition, the equations of the complete explanation of particle's motion are

$$\left(\frac{dr}{ds}\right)^2 = E^2 - f_s(r) \left(\epsilon + \frac{L^2}{r^2}\right), \quad (11)$$

$$\left(\frac{dr}{d\phi}\right)^2 = \frac{r^4}{L^2} \left(E^2 - f_s(r) \left(\epsilon + \frac{L^2}{r^2}\right)\right) =: R(r), \quad (12)$$

$$\left(\frac{dr}{dt}\right)^2 = \frac{f_s^2(r)}{E^2} \left(E^2 - f_s(r) \left(\epsilon + \frac{L^2}{r^2}\right)\right). \quad (13)$$

The effective potential V_{eff} can be get from Eq. (11) as

$$V_{eff} = \left(1 - \frac{2M}{r} + \frac{Q^2}{r^2} - \frac{N_s}{r \frac{1+3\omega_s-6k\lambda(1+\omega_s)}{1-3k\lambda(1+\omega_s)}}\right) \left(\epsilon + \frac{L^2}{r^2}\right). \quad (14)$$

We rewrite the equations with new dimensionless parameters

$$\tilde{r} = \frac{r}{M}, \quad \tilde{L} = \frac{M^2}{L^2}, \quad \tilde{N} = MN, \quad \tilde{Q} = \frac{Q}{M}, \quad (15)$$

so we have

$$ds^2 = -f_s(\tilde{r}) dt^2 + \frac{d\tilde{r}^2}{f_s(\tilde{r})} + \tilde{r}^2 d\Omega^2, \quad (16)$$

$$f_s(\tilde{r}) = 1 - \frac{2}{\tilde{r}} + \frac{\tilde{Q}^2}{\tilde{r}^2} - \frac{\tilde{N}_s}{\tilde{r} \frac{1+3\omega_s-6k\lambda(1+\omega_s)}{1-3k\lambda(1+\omega_s)}}, \quad (17)$$

and the Eq. (12) with the generic metric of Rastall theory (Eq. (7)) takes the following form

$$\left(\frac{d\tilde{r}}{d\phi}\right)^2 = \tilde{r}^4 \tilde{L} \left(E^2 - \left(1 - \frac{2}{\tilde{r}} + \frac{\tilde{Q}^2}{\tilde{r}^2} - \frac{\tilde{N}_s}{\tilde{r} \frac{1+3\omega_s-6k\lambda(1+\omega_s)}{1-3k\lambda(1+\omega_s)}} \right) \left(\epsilon + \frac{1}{\tilde{L}\tilde{r}^2} \right) \right) = R(\tilde{r}). \quad (18)$$

To solve this equation and investigate its results, we study analytical solutions of geodesic equations of a black hole surrounded by quintessence, dust, cosmological constant, radiation and phantom field.

3.1. The black hole surrounded by the quintessence field

In this section, we obtain the equations of motion for two possible values of $k\lambda$ for the quintessence surrounding field. By putting $\omega_s = \omega_q = -\frac{2}{3}$ [50], the Eqs. (16) and (17) convert to the following equations

$$ds^2 = -f_q(\tilde{r})dt^2 + \frac{d\tilde{r}^2}{f_q(\tilde{r})} + \tilde{r}^2 d\Omega^2, \quad (19)$$

$$f_q(\tilde{r}) = 1 - \frac{2}{\tilde{r}} + \frac{\tilde{Q}^2}{\tilde{r}^2} - \frac{\tilde{N}_q}{\tilde{r}^{1-k\lambda}}. \quad (20)$$

The equation of effective state parameter ω_{eff} can be obtained by comparing the Eqs. (19) and (20) with the original Kieslev metric (Eq. (8)) [19]

$$\omega_{eff} = \frac{1}{3} \left(-1 - \frac{1 + 2k\lambda}{1 - k\lambda} \right). \quad (21)$$

By considering two values of $\omega_{eff} \leq -\frac{1}{3}$ and $\omega_{eff} \geq -\frac{1}{3}$ in Eq. (8) [19], the range values of $k\lambda$ in Eq. (21) are discernible as $-\frac{1}{2} \leq k\lambda < 1$ and $k\lambda \leq -\frac{1}{2} \cup k\lambda > 1$ respectively. Of course, in this paper for all surrounding fields cases, we consider the possible values of $k\lambda$, so that $f_s(r)$ in Eq. (17) have included integer powers of r and also Eq. (18) can be solved analytically. For other values of $k\lambda$, Eq. (18) have some terms with fractional powers of \tilde{r} , which in our ability can not be solved analytically but may be solved numerically same as applied technique in Ref. [51].

- For $\omega_{eff} \leq -\frac{1}{3}$ and $k\lambda = \frac{1}{4}$,

the metric (19) can be written as

$$ds^2 = -f_q(\tilde{r})dt^2 + \frac{d\tilde{r}^2}{f_q(\tilde{r})} + \tilde{r}^2 d\Omega^2, \quad (22)$$

$$f_q(\tilde{r}) = 1 - \frac{2}{\tilde{r}} + \frac{\tilde{Q}^2}{\tilde{r}^2} - \tilde{N}_q \tilde{r}^2 \quad (23)$$

and

$$V_{eff} = \left(1 - \frac{2}{\tilde{r}} + \frac{\tilde{Q}^2}{\tilde{r}^2} - \tilde{N}_q \tilde{r}^2 \right) \left(\epsilon + \frac{1}{\tilde{L} \tilde{r}^2} \right). \quad (24)$$

so the Eq. (18) for the quintessence surrounding field, get the following form

$$\left(\frac{d\tilde{r}}{d\varphi} \right)^2 = \tilde{N}_q \epsilon \tilde{L} \tilde{r}^6 + ((E^2 - \epsilon) \tilde{L} + \tilde{N}_q) r^4 + 2\epsilon \tilde{L} \tilde{r}^3 - (1 + \tilde{Q}^2 \epsilon \tilde{L}) \tilde{r}^2 + 2\tilde{r} - \tilde{Q}^2 = R_q(\tilde{r}), \quad (25)$$

- For $\omega_{eff} \geq -\frac{1}{3}$ and $k\lambda = -2$, then

$$ds^2 = -f_q(\tilde{r})dt^2 + \frac{d\tilde{r}^2}{f_q(\tilde{r})} + \tilde{r}^2 d\Omega^2, \quad (26)$$

$$f_q(\tilde{r}) = 1 - \frac{2+\tilde{N}_q}{\tilde{r}} + \frac{\tilde{Q}^2}{\tilde{r}^2}, \quad (27)$$

and

$$V_{eff} = \left(1 - \frac{2+\tilde{N}_q}{\tilde{r}} + \frac{\tilde{Q}^2}{\tilde{r}^2}\right)\left(\epsilon + \frac{1}{\tilde{L}\tilde{r}^2}\right). \quad (28)$$

The Eq. (18) can be written

$$\left(\frac{d\tilde{r}}{d\varphi}\right)^2 = (E^2 - \epsilon)\tilde{L}r^4 + (2 + \tilde{N}_q)\epsilon\tilde{L}\tilde{r}^3 - (1 + \tilde{Q}^2\epsilon\tilde{L})\tilde{r}^2 + (2 + \tilde{N}_q)\tilde{r} - \tilde{Q}^2 = R_q(\tilde{r}), \quad (29)$$

3.1.1. Analytical Solution of Geodesic Equations

In this section, we present the analytical solution of the geodesic Eqs. (25) and (29).

a. Null Geodesics For light ray ($\epsilon = 0$), Eqs. (25) and (29) are polynomials of degree four in the form $\left(\frac{d\tilde{r}}{d\varphi}\right)^2 = \sum_{i=0}^4 a_i r^i$, which by substitution $\tilde{r} = \frac{1}{u} + \tilde{r}_R$, where \tilde{r}_R is a zero of R , convert to a polynomial R_3 of degree 3

$$\left(\frac{du}{d\varphi}\right)^2 = R_3(u) = \sum_{j=1}^3 b_j u^j, \quad u(\phi_0) = u_0, \quad (30)$$

where

$$b_j = \frac{1}{(4-j)!} \frac{d^{(4-j)}R}{d\tilde{r}^{4-j}}(\tilde{r}_R), \quad (31)$$

in which b_j , ($j = 1, 2, 3$) is an arbitrary constant of the relevant metric. Next, substitution $u = \frac{1}{b_3}(4y - \frac{b_2}{3})$, transform $R_3(u)$, to elliptical type differential equation as [49]

$$\left(\frac{dy}{d\phi}\right)^2 = 4y^3 - g_2y - g_3 = p_3(y). \quad (32)$$

Equation (32) known as the Weierstrass form which

$$g_2 = \frac{1}{16}\left(\frac{4}{3}b_2^2 - 4b_1b_3\right), \quad g_3 = \frac{1}{16}\left(\frac{1}{3}b_1b_2b_3 - \frac{2}{27}b_2^3b_3^2\right), \quad (33)$$

are the Weierstrass invariants. So, the answer of Eq. (32), using the Weierstrass function, is as follows

$$y(\phi) = \wp(\phi - \phi_{in}; g_2, g_3), \quad (34)$$

in which $\phi_{in} = \phi_0 + \int_{y_0}^{\infty} \frac{dy}{\sqrt{4y^3 - g_2y - g_3}}$ with $\phi_0 = \frac{1}{4}\left(\frac{b_3}{\tilde{r}_0 - \tilde{r}_R} + \frac{b_2}{3}\right)$ depends only on the initial value ϕ_0 and \tilde{r}_0 . Eventually, the solution of polynomials of degree four is [1]

$$\tilde{r}(\phi) = \frac{b_3}{4\wp(\phi - \phi_{in}; g_2, g_3) - \frac{b_2}{3}} + \tilde{r}_R. \quad (35)$$

This analytic solution is obtained for null geodesic in quintessence surrounding field in Rastall theory and is reliable in all regions of this space-times. The explanation and properties presented in this section are applied to solve all geodesic equations of elliptic type in this paper.

b. Timelike Geodesics For the massive particle ($\epsilon = 1$) Eq. (25) is a polynomial of order six and also of the hyperelliptic type. By substitution $\tilde{r} = \frac{1}{u} + \tilde{r}_R$, where \tilde{r}_R is a zero of R , the equation of motion can be reduced to one of the two forms

$$\left(u \frac{du}{d\phi}\right)^2 = P_5(u), \quad (36)$$

$$\left(\frac{du}{d\phi}\right)^2 = P_5(u). \quad (37)$$

The analytic solution of above equations, which is extensively discussed in [47, 49, 52], is given in form of derivatives of the Kleinian σ function as

$$u(\varphi) = -\frac{\sigma_1(\varphi_\infty)}{\sigma_2(\varphi_\infty)} \Big|_{\sigma(\varphi_\infty)=0}, \quad (38)$$

with

$$\varphi_\infty = (\varphi_2, \varphi - \varphi'_{in}), \quad (39)$$

where $\varphi'_{in} = \varphi_{in} + \int_{\varphi_{in}}^{\infty} \frac{udu'}{\sqrt{P_5(u')}}$. The component φ_2 is determined by the condition $\sigma(\varphi_\infty) = 0$. Also, the function σ_i is the i th derivative of Kleinian σ function and σ_z is

$$\sigma_z = C e^{zt} k z \theta[g, \theta](2w^{-1}z; \tau), \quad (40)$$

where C is a constant, τ is the symmetric Riemann matrix, ω is the period matrix, $k = \eta(2)^{-1}$ which η is the periodmatrix of the second kind and θ is the Riemann function with characteristic $[g, h]$ which $2[g, h] = (0, 1)^t + (1, 1)^t \tau$ [40, 42, 45, 53], So the solution of Eq. (25) becomes

$$r(\varphi) = -\frac{\sigma_2(\varphi_\infty)}{\sigma_1(\varphi_\infty)}. \quad (41)$$

This analytic solution is obtained for timelike geodesic in the quintessence surrounding field in Rastall theory and is reliable in all regions of this space-times. The explanation and properties presented in this section are applied to solve all geodesic equations of hyperelliptic type in this paper.

We use of these analytical solutions to plot some example of possible orbits of test particles

and light ray, but before that we need to plot $\tilde{L} - E^2$ diagram for each cases. Solving $R_q(\tilde{r}) = 0$ and $\frac{dR_q(\tilde{r})}{d\tilde{r}} = 0$ give us E^2 and \tilde{L} equations. For massive particles ($\epsilon = 1$) in a black hole surrounded by the quintessence field with $k\lambda = \frac{1}{4}$, we have

$$\tilde{L} = -\frac{2\tilde{Q}^2 + \tilde{r}^2 - 3\tilde{r}}{\tilde{r}^2(\tilde{N}_q\tilde{r}^4 + \tilde{Q}^2 - r)}, \quad E^2 = \frac{(-\tilde{N}_q\tilde{r}^4 + \tilde{Q}^2 + \tilde{r}^2 - 2\tilde{r})^2}{(2\tilde{Q}^2 + \tilde{r}^2 - 3\tilde{r})\tilde{r}^2}, \quad (42)$$

and for massless particles ($\epsilon = 0$)

$$\tilde{L} = \frac{-\tilde{N}_q\tilde{r}^4 + \tilde{Q}^2 + \tilde{r}^2 - 2\tilde{r}}{E^2\tilde{r}^4}. \quad (43)$$

With $k\lambda = -2$, for massive particle ($\epsilon = 1$)

$$\tilde{L} = -\frac{4\tilde{Q}^2 - 3(2 + \tilde{N}_q)\tilde{r} + 2\tilde{r}^2)^2}{(2\tilde{Q}^2 - \tilde{N}_q\tilde{r} + 2\tilde{r}^2 - 2\tilde{r})\tilde{r}^2}, \quad E^2 = \frac{2(\tilde{Q}^2 - (2 + \tilde{N}_q)\tilde{r} + \tilde{r}^2)^2}{(4\tilde{Q}^2 - 3(2 + \tilde{N}_q)\tilde{r} + 2\tilde{r}^2)\tilde{r}^2}, \quad (44)$$

and for massless particles ($\epsilon = 0$)

$$\tilde{L} = \frac{\tilde{Q}^2 + \tilde{r}^2 - (2 + \tilde{N}_q)\tilde{r}}{E^2\tilde{r}^4}. \quad (45)$$

Figures of $\tilde{L} - E^2$ diagrams (Eqs. (42)-(45)) have been shown in Figs. 1 and 3. Moreover, a summary of possible orbits type with numbers of zero points in each regions for both cases $k\lambda = \frac{1}{4}$ and $k\lambda = -2$ are shown in table I and II respectively. Also results of timelike and null geodesic effective potential (Eqs. (24), (28)) are shown in Figs. 2 and 4.

3.2. The black hole surrounded by dust field

When the black hole is surrounded by the dust field, we put $\omega_s = \omega_d = 0$ [50] and the metric (16) writes as follows

$$ds^2 = -f_d(\tilde{r})dt^2 + \frac{d\tilde{r}^2}{f_d(\tilde{r})} + \tilde{r}^2d\Omega^2, \quad (46)$$

$$f_d(\tilde{r}) = 1 - \frac{2}{\tilde{r}} + \frac{\tilde{Q}_d^2}{\tilde{r}^2} - \frac{\tilde{N}_d}{\tilde{r}^{1-3k\lambda}}. \quad (47)$$

The equation of effective state parameter ω_{eff} can be obtained by comparing this metric with the original Kieslev metric (8), as [19]

$$\omega_{eff} = \frac{1}{3}\left(-1 + \frac{1 - 6k\lambda}{1 - 3k\lambda}\right). \quad (48)$$

By considering two values of $\omega_{eff} \leq -\frac{1}{3}$ and $\omega_{eff} \geq -\frac{1}{3}$ in Eq. (8) [19], the range values of $k\lambda$ in Eq. (48) are discernible as $\frac{1}{6} < k\lambda < \frac{1}{3}$ and $k\lambda < \frac{1}{6} \cup k\lambda > \frac{1}{3}$ respectively. To solving the analytical solution of the equations of motion for surrounding dust field

- we consider $k\lambda = \frac{2}{9}$ for $\omega_{eff} \leq -\frac{1}{3}$,

so the metric (46) can be written as

$$ds^2 = -f_d(\tilde{r})dt^2 + \frac{d\tilde{r}^2}{f_d(\tilde{r})} + \tilde{r}^2 d\Omega^2, \quad (49)$$

$$f_d(\tilde{r}) = 1 - \frac{2}{\tilde{r}} + \frac{\tilde{Q}^2}{\tilde{r}^2} - \tilde{N}_d \tilde{r} \quad (50)$$

and

$$V_{eff} = \left(1 - \frac{2}{\tilde{r}} + \frac{\tilde{Q}^2}{\tilde{r}^2} - \tilde{N}_d \tilde{r}\right) \left(\epsilon + \frac{1}{\tilde{L}\tilde{r}^2}\right). \quad (51)$$

Then the metric (18) get the form

$$\left(\frac{d\tilde{r}}{d\varphi}\right)^2 = \tilde{N}_d \epsilon \tilde{L} \tilde{r}^5 + (E^2 - \epsilon) \tilde{L} r^4 + (2\tilde{L}\epsilon + \tilde{N}_d) \tilde{r}^3 - (1 + \tilde{Q}^2 \epsilon \tilde{L}) \tilde{r}^2 + 2\tilde{r} - \tilde{Q}^2 = R_d(\tilde{r}), \quad (52)$$

For $\epsilon = 0$, Eq. (52) is of elliptic type and therefore has analytical solution same as Sec. 3.1.1(a)

$$\tilde{r}(\phi) = \frac{b_3}{4\wp(\phi - \phi_{in}; g_2, g_3) - \frac{b_2}{3}} + \tilde{r}_R. \quad (53)$$

But for $\epsilon = 1$, Eq. (52) is of hyperelliptic type, therefore has analytical solution same as Sec. 3.1.1(b)

$$\tilde{r}(\varphi) = -\frac{\sigma_2(\varphi_\infty)}{\sigma_1(\varphi_\infty)} \quad (54)$$

- Our next possible choice is $k\lambda = \frac{1}{4}$, with $\omega_{eff} \geq -\frac{1}{3}$,

so the metric (46) can be written as

$$ds^2 = -f_d(\tilde{r})dt^2 + \frac{d\tilde{r}^2}{f_d(\tilde{r})} + \tilde{r}^2 d\Omega^2, \quad (55)$$

$$f_d(\tilde{r}) = 1 - \frac{2}{\tilde{r}} + \frac{\tilde{Q}^2}{\tilde{r}^2} - \tilde{N}_d \tilde{r}^2, \quad (56)$$

with the effective potential

$$V_{eff} = \left(1 - \frac{2}{\tilde{r}} + \frac{\tilde{Q}^2}{\tilde{r}^2} - \tilde{N}_d \tilde{r}^2\right) \left(\epsilon + \frac{1}{\tilde{L}\tilde{r}^2}\right). \quad (57)$$

then

$$\left(\frac{d\tilde{r}}{d\varphi}\right)^2 = \tilde{N}_d \epsilon \tilde{L} \tilde{r}^6 + ((E^2 - \epsilon) \tilde{L} + \tilde{N}_d) r^4 + 2\tilde{L} \epsilon \tilde{r}^3 - (1 + \tilde{Q}^2 \epsilon \tilde{L}) \tilde{r}^2 + 2\tilde{r} - \tilde{Q}^2 = R_d(\tilde{r}), \quad (58)$$

In order to obtain the analytical solution, for $\epsilon = 0$, Eq. (58) is of elliptic type which has analytical solution same as Sec. 3.1.1(a)

$$\tilde{r}(\phi) = \frac{b_3}{4\wp(\phi - \phi_{in}; g_2, g_3) - \frac{b_2}{3}} + \tilde{r}_R. \quad (59)$$

But for $\epsilon = 1$, the analytical solution of Eq. (58) is similar to Sec. 3.1.1(b)

$$\tilde{r}(\varphi) = -\frac{\sigma_2(\varphi_\infty)}{\sigma_1(\varphi_\infty)} \quad (60)$$

In next, as discussed in the previous section, we need to plot $\tilde{L} - E^2$ diagram. So by solving $R_d(\tilde{r}) = 0$ and $\frac{dR_d(\tilde{r})}{d\tilde{r}} = 0$ for massive particles ($\epsilon = 1$) with $k\lambda = \frac{2}{9}$

$$\tilde{L} = -\frac{-\tilde{N}_d\tilde{r}^3 + 4\tilde{Q}^2 + 2\tilde{r}^2 - 6\tilde{r}}{\tilde{r}^2(\tilde{N}_d\tilde{r}^3 + 2\tilde{Q}^2 - 2\tilde{r})}, \quad E^2 = \frac{2(-\tilde{N}_d\tilde{r}^3 + \tilde{Q}^2 + \tilde{r}^2 - 2\tilde{r})^2}{(-\tilde{N}_d\tilde{r}^3 + 4\tilde{Q}^2 + 2\tilde{r}^2 - 6\tilde{r})\tilde{r}^2}, \quad (61)$$

and for massless particles ($\epsilon = 0$)

$$\tilde{L} = -\frac{-\tilde{N}_d\tilde{r}^3 + \tilde{Q}^2 + \tilde{r}^2 - 2\tilde{r}}{E^2\tilde{r}^4}. \quad (62)$$

The figures of $\tilde{L} - E^2$ diagram (Eqs. (61)-(62)) with the region of different types of geodesic motion in the dust surrounding field with the case $k\lambda = \frac{2}{9}$, has been illustrated in Fig. 5 while $\tilde{L} - E^2$ diagram for the case $k\lambda = \frac{1}{4}$ are identical with the same case in the quintessence surrounding field (Figs. 1, 2). Moreover, a summary of possible orbits type with numbers of zero points in each region is shown in table III. Also results of timelike and null geodesic effective potential (Eqs. (51), (57)) has been shown in Fig. 6.

3.3. The black hole surrounded by the Radiation field

When the radiation is surrounding field, we put $w_r = \frac{1}{3}$ [50], so the metric (16) can be written as

$$ds^2 = -f_r(\tilde{r})dt^2 + \frac{d\tilde{r}^2}{f_r(\tilde{r})} + \tilde{r}^2d\Omega^2, \quad (63)$$

$$f_r(\tilde{r}) = 1 - \frac{2}{\tilde{r}} + \frac{\tilde{Q}^2 - \tilde{N}_r}{\tilde{r}^2}, \quad (64)$$

with the effective potential

$$V_{eff} = \left(1 - \frac{2}{\tilde{r}} + \frac{\tilde{Q}^2 - \tilde{N}_r}{\tilde{r}^2}\right)\left(\epsilon + \frac{1}{\tilde{L}\tilde{r}^2}\right). \quad (65)$$

The metric (63) is the Reissner-Nordström metric of a black hole with an effective charge $Q_{eff} = \sqrt{\tilde{Q}^2 - \tilde{N}_r}$. Due to the similarity of the metric of a black hole surrounded by the radiation field (Eq. (63)) with GR, the geometric effects of the Rastall parameters do not observe. Therefore the Eq. (18) for the black hole surrounded by the Radiation field becomes

$$\left(\frac{d\tilde{r}}{d\varphi}\right)^2 = (E^2 - \epsilon)\tilde{L}\tilde{r}^4 + 2\epsilon\tilde{L}\tilde{r}^3 - ((\tilde{Q}^2 - \tilde{N}_r)\epsilon\tilde{L} + 1)\tilde{r}^2 + 2\tilde{r} - (\tilde{Q}^2 - \tilde{N}_r) = R_r(\tilde{r}), \quad (66)$$

which for both massive and massless particles has analytical solution similar to Sec. 3.1.1(a)

$$\tilde{r}(\phi) = \frac{b_3}{4\wp(\phi - \phi_{in}; g_2, g_3) - \frac{b_2}{3}}. \quad (67)$$

To plot $\tilde{L} - E^2$ diagram for a black hole surrounded by the radiation field, by solving $R_r(\tilde{r}) = 0$ and $\frac{dR_r(\tilde{r})}{d\tilde{r}} = 0$, for massive particles ($\epsilon = 1$) we have

$$\tilde{L} = -\frac{2(\tilde{Q}^2 - \tilde{N}_r) + \tilde{r}^2 - 3\tilde{r}}{\tilde{r}^2((\tilde{Q}^2 - \tilde{N}_r) - \tilde{r})}, \quad E^2 = \frac{((\tilde{Q}^2 - \tilde{N}_r) + \tilde{r}^2 - 2\tilde{r})^2}{(2(\tilde{Q}^2 - \tilde{N}_r) + \tilde{r}^2 - 3\tilde{r})\tilde{r}^2}, \quad (68)$$

and for massless particles ($\epsilon = 0$)

$$\tilde{L} = \frac{(\tilde{Q}^2 - \tilde{N}_r) + \tilde{r}^2 - 2\tilde{r}}{E^2\tilde{r}^4}. \quad (69)$$

The figures of $\tilde{L} - E^2$ diagrams (Eqs. (68)-(69)) with the region of different types of geodesic motion, in the radiation surrounding field, have been shown in Fig. 7. Also plots of effective potential (Eq. (65)) is shown in Fig. 8. Moreover, a summary of possible orbits type with numbers of zero points in each regions for both massive and massless particles is shown in table IV.

3.4. The black hole surrounded by the cosmological constant field

For the cosmological constant surrounding field, we put $w_c = -1$ [50], so the metric (16) can be written as

$$ds^2 = -f_c(\tilde{r})dt^2 + \frac{d\tilde{r}^2}{f_c(\tilde{r})} + \tilde{r}^2 d\Omega^2, \quad (70)$$

$$f_c(\tilde{r}) = 1 - \frac{2}{\tilde{r}} + \frac{\tilde{Q}^2}{\tilde{r}^2} - \tilde{N}_c\tilde{r}^2 \quad (71)$$

with effective potential

$$V_{eff} = \left(1 - \frac{2}{\tilde{r}} + \frac{\tilde{Q}^2}{\tilde{r}^2} - \tilde{N}_c\tilde{r}^2\right)\left(\epsilon + \frac{1}{\tilde{L}\tilde{r}^2}\right). \quad (72)$$

so the Eq. (18) gets the form

$$\left(\frac{d\tilde{r}}{d\varphi}\right)^2 = \tilde{N}_c \epsilon \tilde{L} \tilde{r}^6 + ((E^2 - \epsilon)\tilde{L} + \tilde{N}_c)r^4 + 2\tilde{L}\epsilon\tilde{r}^3 - (1 + \tilde{Q}^2\epsilon\tilde{L})\tilde{r}^2 + 2\tilde{r} - \tilde{Q}^2 = R_c(\tilde{r}), \quad (73)$$

The analytical solution of (73) for massive particles ($\epsilon = 1$), is same as Sec. 3.1.1(b)

$$r(\varphi) = -\frac{\sigma_2(\varphi_\infty)}{\sigma_1(\varphi_\infty)} \quad (74)$$

and to solve null geodesics ($\epsilon = 0$), Eq. (73) is a polynomial of degree four, which has analytical solution like Sec. 3.1.1(a)

$$\tilde{r}(\phi) = \frac{b_3}{4\wp(\phi - \phi_{in}; g_2, g_3) - \frac{b_2}{3}} + \tilde{r}_R. \quad (75)$$

Due to exact similarity of Eq. (73) with Eq. (25) in the quintessence surrounding field, except with difference between coefficient, solving $R_c(\tilde{r}) = 0$ and $\frac{dR_c(\tilde{r})}{d\tilde{r}} = 0$, give us E^2 and \tilde{L} diagram similar to the quintessence surrounding field (Sec. 3.1.1(a), 3.1.1(b)). Thus for massive particles ($\epsilon = 1$) in the black hole surrounded by the cosmological constant surrounding field, we have

$$\tilde{L} = -\frac{2\tilde{Q}^2 + \tilde{r}^2 - 3\tilde{r}}{\tilde{r}^2(\tilde{N}_c\tilde{r}^4 + \tilde{Q}^2 - \tilde{r})}, \quad E^2 = \frac{(-\tilde{N}_c\tilde{r}^4 + \tilde{Q}^2 + \tilde{r}^2 - 2\tilde{r})^2}{(2\tilde{Q}^2 + \tilde{r}^2 - 3\tilde{r})\tilde{r}^2}, \quad (76)$$

and for massless particles ($\epsilon = 0$)

$$\tilde{L} = \frac{-\tilde{N}_c\tilde{r}^4 + \tilde{Q}^2 + \tilde{r}^2 - 2\tilde{r}}{E^2\tilde{r}^4}. \quad (77)$$

Therefore figures of $\tilde{L} - E^2$ diagram (Eqs. (76), (77)) for the black hole surrounded by the cosmological constant background, are like the quintessence and also the dust surrounding field (with $k\lambda = \frac{1}{4}$), which has been shown in Figs. 1 and 5. Also results of timelike and null geodesic effective potential Eq. (72) is same as the figure of the quintessence surrounding field, which is shown in Fig. 2.

3.5. The black hole surrounded by the phantom field

For the phantom surrounding field, we put $\omega_c = -\frac{4}{3}$ [50], so the metric (16) can be obtained as

$$ds^2 = -f_p(\tilde{r})dt^2 + \frac{d\tilde{r}^2}{f_p(\tilde{r})} + \tilde{r}^2 d\Omega^2, \quad (78)$$

$$f_p(\tilde{r}) = 1 - \frac{2}{\tilde{r}} + \frac{\tilde{Q}^2}{\tilde{r}^2} - \frac{\tilde{N}_p}{\tilde{r}^{1+k\lambda}}. \quad (79)$$

The equation of effective state parameter ω_{eff} can be obtained by comparing the Eq. (78) with the Kieslev metric (8) [19]

$$\omega_{eff} = \frac{1}{3} \left(-1 - \frac{3 - 2k\lambda}{1 + k\lambda} \right). \quad (80)$$

Now by considering two values of $\omega_{eff} \leq -\frac{1}{3}$ and $\omega_{eff} \geq -\frac{1}{3}$ in Eq. (8) [19], the range values of $k\lambda$ in Eq. (80) are discernible as $-1 \leq k\lambda < \frac{3}{2}$ and $k\lambda \leq -1 \cup k\lambda \geq \frac{3}{2}$ respectively. In following, we consider these range values of $k\lambda$ to solving the analytical solution of the equations of motion,

- In the range $\omega_{eff} \leq -\frac{1}{3}$, for $k\lambda = \frac{2}{3}$, we have

$$ds^2 = -f_p(\tilde{r})dt^2 + \frac{d\tilde{r}^2}{f_p(\tilde{r})} + \tilde{r}^2 d\Omega^2, \quad (81)$$

$$f_p(\tilde{r}) = 1 - \frac{2}{\tilde{r}} + \frac{\tilde{Q}^2}{\tilde{r}^2} - \tilde{N}_p \tilde{r}, \quad (82)$$

with effective potential

$$V_{eff} = \left(1 - \frac{2}{\tilde{r}} + \frac{\tilde{Q}^2}{\tilde{r}^2} - \tilde{N}_p \tilde{r} \right) \left(\epsilon + \frac{1}{\tilde{L}\tilde{r}^2} \right), \quad (83)$$

so the Eq. (18) get the form

$$\left(\frac{d\tilde{r}}{d\varphi} \right)^2 = \tilde{N}_p \epsilon \tilde{L} \tilde{r}^5 + (E^2 - \epsilon) \tilde{L} \tilde{r}^4 + (2\tilde{L}\epsilon + \tilde{N}_p) \tilde{r}^3 - (1 + \tilde{Q}^2 \epsilon \tilde{L}) \tilde{r}^2 + 2\tilde{r} - \tilde{Q}^2 = R_p(\tilde{r}), \quad (84)$$

Eq. (84) is exactly similar to massive case $k\lambda = \frac{2}{9}$ in the dust surrounding field (Eq. (52)), except with difference between metric coefficient. Thus the analytical solution for $\epsilon = 0$ is same as Sec. 3.1.1(a) Weierstrass form Eq. (35)

$$\tilde{r}(\phi) = \frac{b_3}{4\wp(\phi - \phi_{in}; g_2, g_3) - \frac{b_2}{3}} + \tilde{r}_R. \quad (85)$$

and for $\epsilon = 1$, Eq. (84) is of order five which answer is the same as Sec. 3.1.1(b)

$$\tilde{r}(\varphi) = -\frac{\sigma_2(\varphi_\infty)}{\sigma_1(\varphi_\infty)}. \quad (86)$$

- In the range of $\omega_{eff} \geq -\frac{1}{3}$, for $k\lambda = \frac{1}{4}$,

$$ds^2 = -(f_p(\tilde{r}))dt^2 + \frac{d\tilde{r}^2}{f_p(\tilde{r})} + \tilde{r}^2 d\Omega^2, \quad (87)$$

$$f_p(\tilde{r}) = 1 - \frac{2}{\tilde{r}} + \frac{\tilde{Q}^2}{\tilde{r}^2} - \tilde{N}_p \tilde{r}^2, \quad (88)$$

with effective potential

$$V_{eff} = \left(1 - \frac{2}{\tilde{r}} + \frac{\tilde{Q}^2}{\tilde{r}^2} - \tilde{N}_p \tilde{r}^2\right) \left(\epsilon + \frac{1}{\tilde{L} \tilde{r}^2}\right), \quad (89)$$

and

$$\left(\frac{d\tilde{r}}{d\varphi}\right)^2 = \tilde{N}_p \epsilon \tilde{L} \tilde{r}^6 + ((E^2 - \epsilon) \tilde{L} + \tilde{N}_p) r^4 + (2\tilde{L}\epsilon) \tilde{r}^3 - (1 + \tilde{Q}^2 \epsilon \tilde{L}) \tilde{r}^2 + 2\tilde{r} - \tilde{Q}^2 = R_p(\tilde{r}), \quad (90)$$

Eq. (90) is similar to Eq. (25) in quintessence and also like Eq. (58) in the dust surrounding field. Thus the analytical solutions are same as Sec. 3.1.1(a) for massless and Sec. 3.1.1(b) for massive geodesic.

- The next possible value in the range $\omega_{eff} \geq -\frac{1}{3}$ is $k\lambda = 4$,

So, the metric (18) will be as the form

$$ds^2 = -f_p(\tilde{r}) dt^2 + \frac{d\tilde{r}^2}{f_p(\tilde{r})} + \tilde{r}^2 d\Omega^2, \quad (91)$$

$$f_p(\tilde{r}) = 1 - \frac{2 + \tilde{N}_p}{\tilde{r}} + \frac{\tilde{Q}^2}{\tilde{r}^2}, \quad (92)$$

with effective potential

$$V_{eff} = \left(1 - \frac{2 + \tilde{N}_p}{\tilde{r}} + \frac{\tilde{Q}^2}{\tilde{r}^2}\right) \left(\epsilon + \frac{1}{\tilde{L} \tilde{r}^2}\right), \quad (93)$$

then

$$\left(\frac{d\tilde{r}}{d\varphi}\right)^2 = (E^2 - \epsilon) \tilde{L} r^4 + (\tilde{N}_p \epsilon + 2\epsilon) \tilde{L} \tilde{r}^3 - (1 + \tilde{Q}^2 \epsilon \tilde{L}) \tilde{r}^2 + 2\tilde{r} + \tilde{N}_p \tilde{r} - \tilde{Q}^2 = R_p(\tilde{r}), \quad (94)$$

Analytical solution of the Eq. (94) for both massive and massless geodesic is given by Weierstrass form same as Sec 3.1.1(a).

For a phantom surrounding field with $k\lambda = 4$, solving $R_p(\tilde{r}) = 0$ and $\frac{dR_p(\tilde{r})}{d\tilde{r}} = 0$ give us $\tilde{L} - E^2$ diagram similar to the case $k\lambda = -2$ in quintessence surrounding field. So for massive particles ($\epsilon = 1$)

$$\tilde{L} = -\frac{4\tilde{Q}^2 + 2\tilde{r}^2 - 3(2 + \tilde{N}_p)\tilde{r}}{\tilde{r}^2(2\tilde{Q}^2 - (2 + \tilde{N}_p)\tilde{r})}, \quad E^2 = \frac{2(\tilde{Q}^2 + \tilde{r}^2 - (2 + \tilde{N}_p)\tilde{r})^2}{(4\tilde{Q}^2 + 2\tilde{r}^2 - 3(2 + \tilde{N}_p)\tilde{r})\tilde{r}^2}, \quad (95)$$

and for massless particles ($\epsilon = 0$)

$$\tilde{L} = \frac{(\tilde{Q}^2 + \tilde{r}^2 - (2 + \tilde{N}_p)\tilde{r})}{E^2 \tilde{r}^4}. \quad (96)$$

Therefore the figures of $\tilde{L} - E^2$ diagram (Eqs. (95), (96)) with the region of different types of geodesic motion in the phantom surrounding field, has been shown in Fig. 9. Also plots of effective potential (Eq. (93)) is shown in Fig. 10. Moreover, a summary of possible orbits type with numbers of zero points in each region are shown in table V.

4. ORBITS

In this section, we use the analysis provided in the previous sections for geodesic equations as well as their analytical solutions, $\tilde{L} - E^2$ diagrams and also effective potential to plot some examples of possible orbit and study some astrophysical applications. So we begin with introducing different types of possible orbits. Suppose \tilde{r}_- be the inner horizon and \tilde{r}_+ be the outer event horizon.

1. *Terminating orbit* (TO) with ranges either $\tilde{r} \in [0, \infty)$ or $\tilde{r} \in [0, r_1)$ with $r_1 \geq r_+$.
2. *Escape orbit* (EO) with range $\tilde{r} \in [r_1, \infty)$ with $r_1 > \tilde{r}_+$.
3. *Bound orbit* (BO) with range $\tilde{r} \in [r_1, r_2]$ with
 - (a) $r_1, r_2 > r_+$, or
 - (b) $0 < r_1, r_2 < r_-$.
4. *Two-world escape orbit* (TEO) with range $[r_1, \infty)$ where $0 < r_1 < r_-$.
5. *Many-world bound orbit* (MBO) with range $\tilde{r} \in [r_1, r_2]$ where $0 < r_1 \leq r_-$ and $r_2 \geq r_+$.

For a certain parameters (E, L, Q, N), different type of orbit is dependent on primary location of the test particle or light ray, for example see Figs. 13(b) and 12(b). In the following, we explain the possible orbit types and examples of effective potentials.

1. In Region O, there is no real positive zero, so the possible type of orbit is TO [see fig. 15].
2. In region I, there is one real positive zero and the kind of possible orbit is TEO [see figs. 12 (b) and 13 (b)].
3. In region II, there are two real positive zeros, therefore the kind of possible orbit is MBO [see figs. 12 (a), 13 (d) and 14 (a)].
4. In region III, there are three real and positive zeros, therefore the kind of two possible orbits are EO [see fig. 13 (a)] and MBO [see figs. 12 (a), 13 (d) and 14 (a)].
5. In region IV, there are four real and positive zeros, so the kind of two possible orbits are BO [see figs. 13 (c), 14 (b)] and MBO [see figs. 12 (a), 13 (d) and 14 (a)].

6. In region V, there are five real and positive zeros, so the kind of three possible orbits are EO [see fig. 13 (a)], BO [see figs. 13 (c), 14 (b)] and MBO [see figs. 12 (a), 13 (d) and 14 (a)].

1. Quintessence surrounding field (with $k\lambda = \frac{1}{4}$)

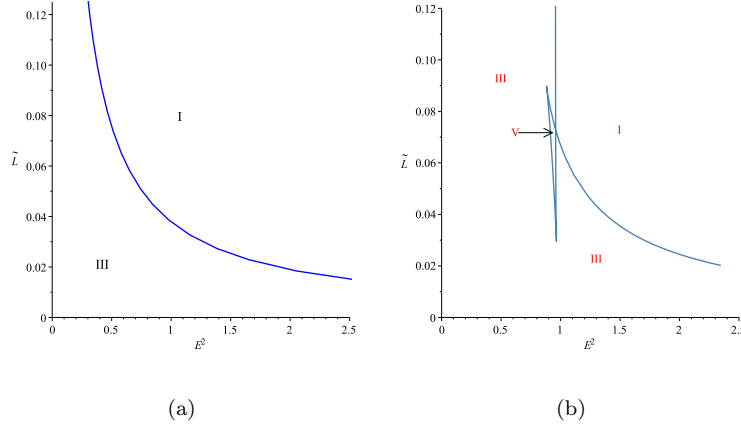


FIG. 1: Plots of $L - E^2$ diagram and regions of different types of geodesic motion in quintessence surrounding field with the parameters $\tilde{N} = \frac{1}{3 \cdot 10^5}$, $\tilde{Q} = \sqrt{0.25}$ for (a): Null geodesic ($\epsilon = 0$) and (b): Timelike geodesic ($\epsilon = 1$). The numbers of positive real zeros in these regions are: I=1, III=3, V=5.

region	pos.zeros	range of \tilde{r}	orbit
I	1		TEO
III	3		MBO, EO
V	5		MBO, BO, EO

TABLE I: Types of orbits of the quintessence surrounding field for $k\lambda = \frac{1}{4}$. The range of the orbits is represented by thick lines. The dots show the turning points of the orbits. The positions of the two horizons are marked by a vertical double line. The single vertical line indicates the singularity at $\tilde{r} = 0$.

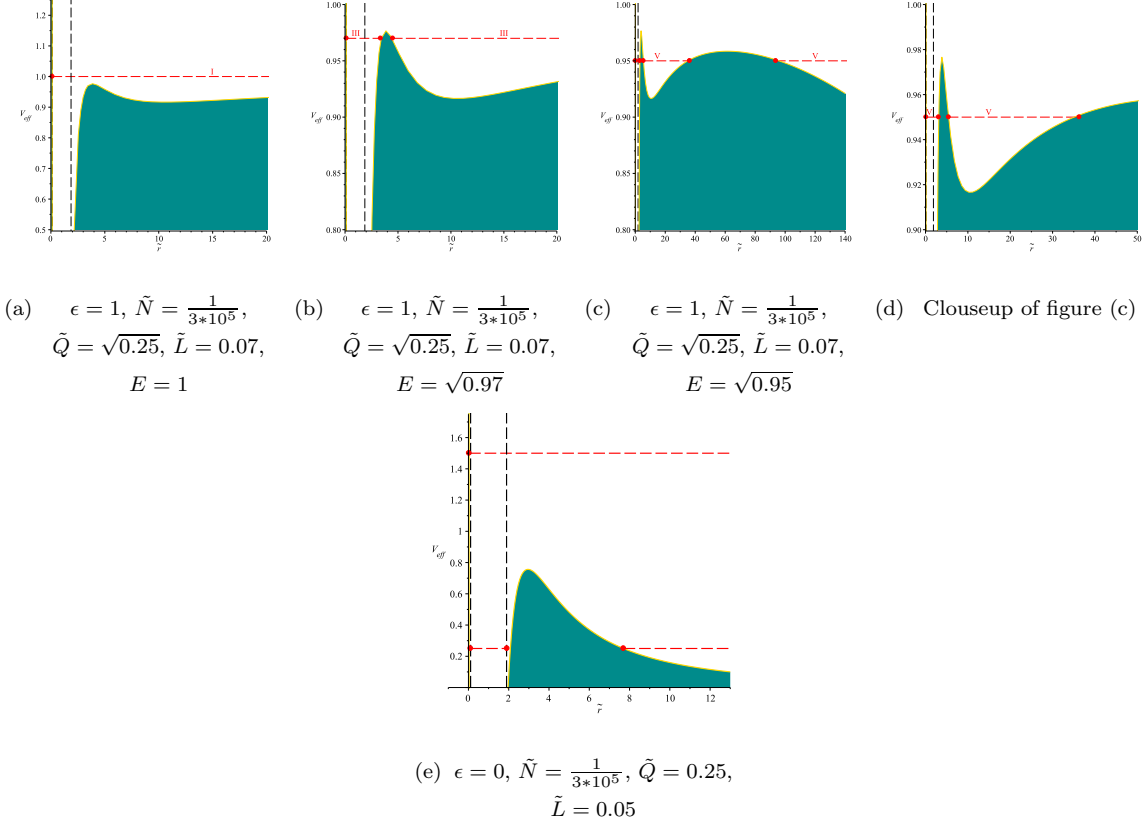


FIG. 2: Plots of the effective potential for the different orbit types of Table I, for the case of quintessence surrounding field with the parameters $k\lambda = \frac{1}{4}$. The horizontal red-dashed lines denotes the squared energy parameter E^2 . The vertical black dashed lines show the position of the horizons. The red dots marks denote the zeros of the polynomial R , which are the turning points of the orbits. In the cyan area, no motion is possible since $\tilde{R} < 0$.

2. Quintessence surrounding field (with $k\lambda = -2$)

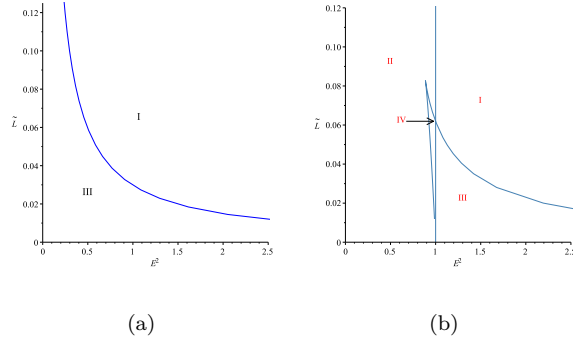


FIG. 3: Plots of $L - E^2$ diagram and region of different types of geodesic motion in a quintessence surrounding field with the parameters $k\lambda = -2$, $\tilde{N} = 0.025$ and $\tilde{Q} = \sqrt{0.25}$ corresponding to table II for (a): Null and (b): Timelike geodesic. The numbers of positive real zeros in these regions are: I=1, II=2, III=3, IV=4.

region	pos.zeros	range of \tilde{r}	orbit
I	1		TEO
II	2		MBO
III	3		MBO, EO
IV	4		MBO, BO

TABLE II: Types of orbits of the quintessence surrounding field for $k\lambda = -2$. The range of the orbits is represented by thick lines. The dots show the turning points of the orbits. The positions of the two horizons are marked by a vertical double line. The single vertical line indicates the singularity at $\tilde{r} = 0$.

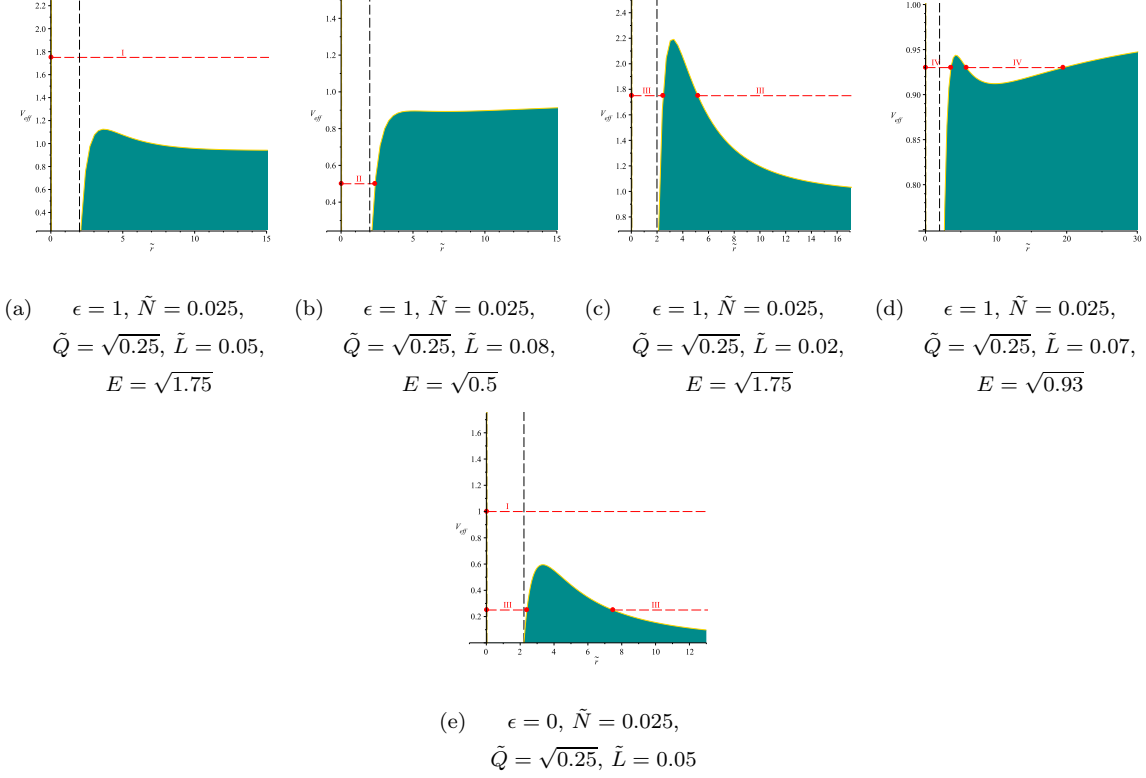


FIG. 4: Plots of the effective potential for the different orbit types of Table II, for the case of quintessence surrounding field with the parameters $k\lambda = -2$. The horizontal red-dashed lines denotes the squared energy parameter E^2 . The vertical black dashed lines show the position of the horizons. The red dots marks denote the zeros of the polynomial R , which are the turning points of the orbits. In the cyan area, no motion is possible since $\tilde{R} < 0$.

3. Dust surrounding field (with $k\lambda = \frac{2}{9}$)

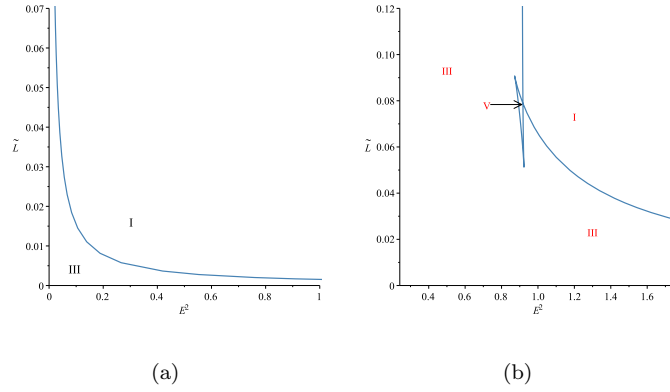
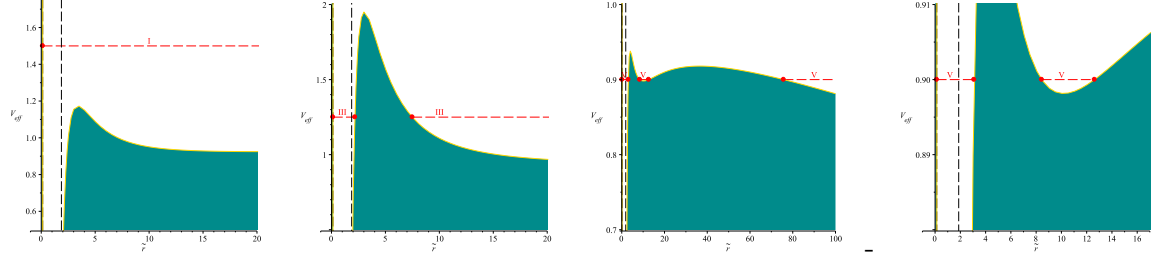


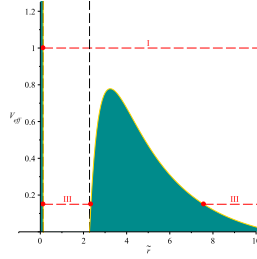
FIG. 5: Plots of $L - E^2$ diagram and region of different types of geodesic motion for the dust surrounding field with the parameters $k\lambda = \frac{2}{9}$, $\tilde{N} = 10^{-3}$, $\tilde{Q} = 0.2$ corresponding to table III for (a): Null geodesic and (b): Timelike geodesic. The numbers of positive real zeros in these regions are: I=1, III=3, V=5.

region	pos.zeros	range of \tilde{r}	orbit
I	1		TEO
III	3		MBO, EO
V	5		MBO, BO, EO

TABLE III: Types of orbits for the dust surrounding field for the case $k\lambda = \frac{2}{9}$. The range of the orbits is represented by thick lines. The dots show the turning points of the orbits. The positions of the two horizons are marked by a vertical double line. The single vertical line indicates the singularity at $\tilde{r} = 0$.



- (a) $\epsilon = 1, \tilde{N} = 10^{-3},$
 $\tilde{Q} = \sqrt{0.25}, \tilde{L} = 0.05,$
 $E = \sqrt{1.5}$
- (b) $\epsilon = 1, \tilde{N} = 10^{-3},$
 $\tilde{Q} = \sqrt{0.25}, \tilde{L} = 0.025,$
 $E = \sqrt{1.25}$
- (c) $\epsilon = 1, \tilde{N} = 10^{-3},$
 $\tilde{Q} = \sqrt{0.25}, \tilde{L} = 0.075,$
 $E = \sqrt{0.9}$
- (d) Cluseup of figure (c)



- (e) $\epsilon = 0, \tilde{N} = 0.075,$
 $\tilde{Q} = \sqrt{0.25}, \tilde{L} = 0.02$

FIG. 6: Plots of the effective potential for the different orbit types of Table III, for the case of dust surrounding field with the parameters $k\lambda = \frac{2}{9}$. The horizontal red-dashed lines denotes the squared energy parameter E^2 . The vertical black dashed lines show the position of the horizons. The red dots marks denote the zeros of the polynomial R , which are the turning points of the orbits. In the cyan area, no motion is possible since $\tilde{R} < 0$.

4. Radiation surrounding field

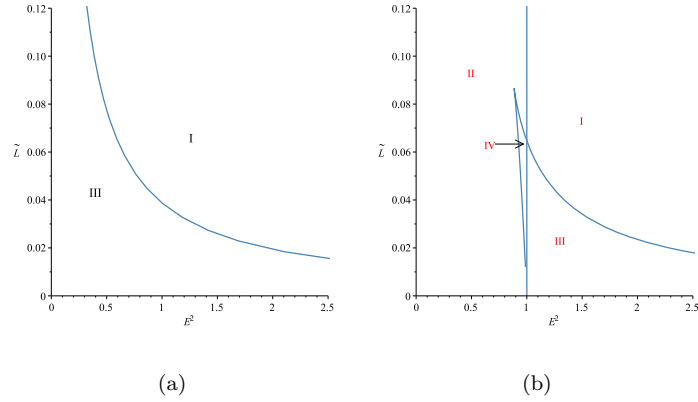


FIG. 7: Plots of $L - E^2$ diagram and regions of different types of geodesic motion for a black hole surrounded by radiation field with the parameters $\tilde{N} = 0.12$ and $\tilde{Q} = \sqrt{0.25}$ corresponding to table IV for (a): Null ($\epsilon = 0$) and (b): Timelike geodesics ($\epsilon = 1$). The numbers of positive real zeros in these regions are: I=1, II=2, III=3, IV=4.

region	pos.zeros	range of \tilde{r}	orbit
I	1		TEO
II	2		MBO
III	3		MBO, EO
IV	4		MBO, BO

TABLE IV: Types of orbits of the radiation surrounding field. The range of the orbits is represented by thick lines. The dots show the turning points of the orbits. The positions of the two horizons are marked by a vertical double line.

The single vertical line indicates the singularity at $\tilde{r} = 0$.

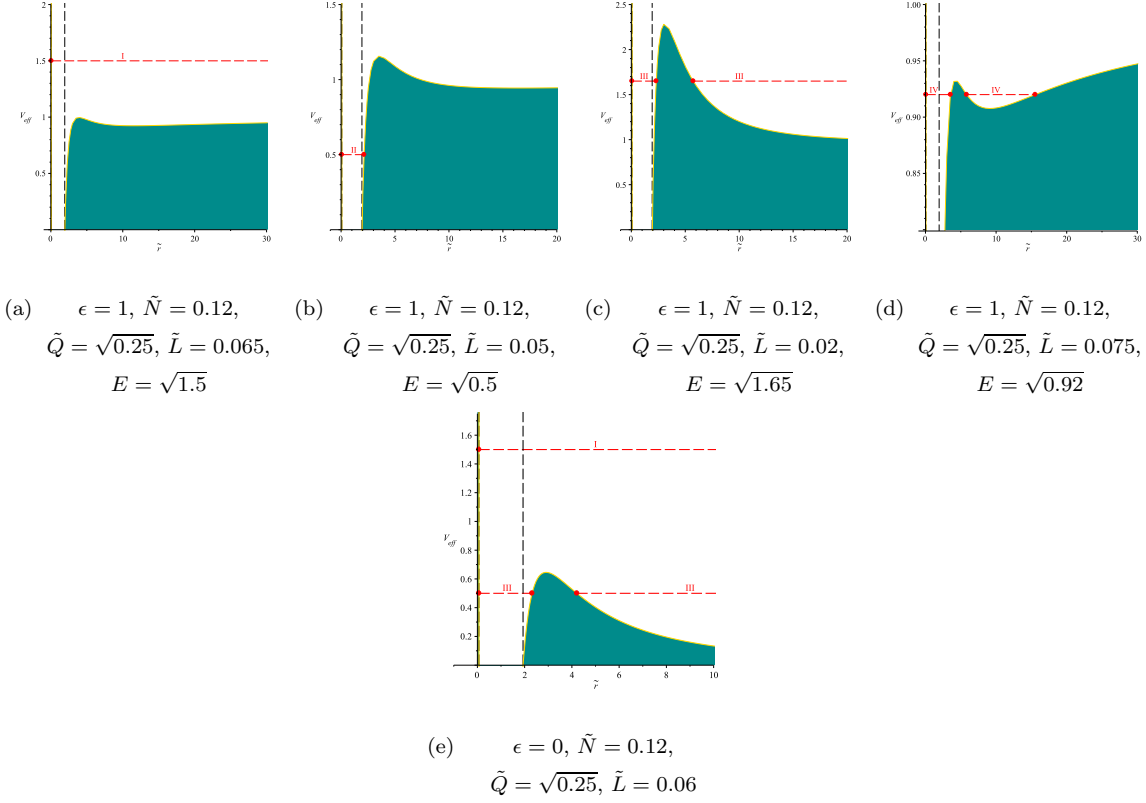


FIG. 8: Plots of the effective potential for the different orbit types of Table IV, for the case of radiation surrounding field. The horizontal red-dashed lines denotes the squared energy parameter E^2 . The vertical black dashed lines show the position of the horizons. The red dots marks denote the zeros of the polynomial R , which are the turning points of the orbits. In the cyan area, no motion is possible since $\tilde{R} < 0$.

5. Phantom surrounding field (with $k\lambda = 4$)

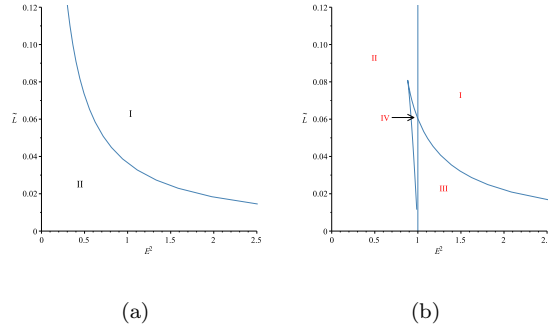


FIG. 9: Plots of $L - E^2$ diagram and region of different types of geodesic motion in the phantom surrounding field with the parameters $k\lambda = 4$, $\tilde{N} = 0.1$ and $\tilde{Q} = \sqrt{0.25}$ (a): Null and (b): Timelike geodesics. The numbers of positive real zeros in these regions are: I=1, II=2, III=3, IV=4.

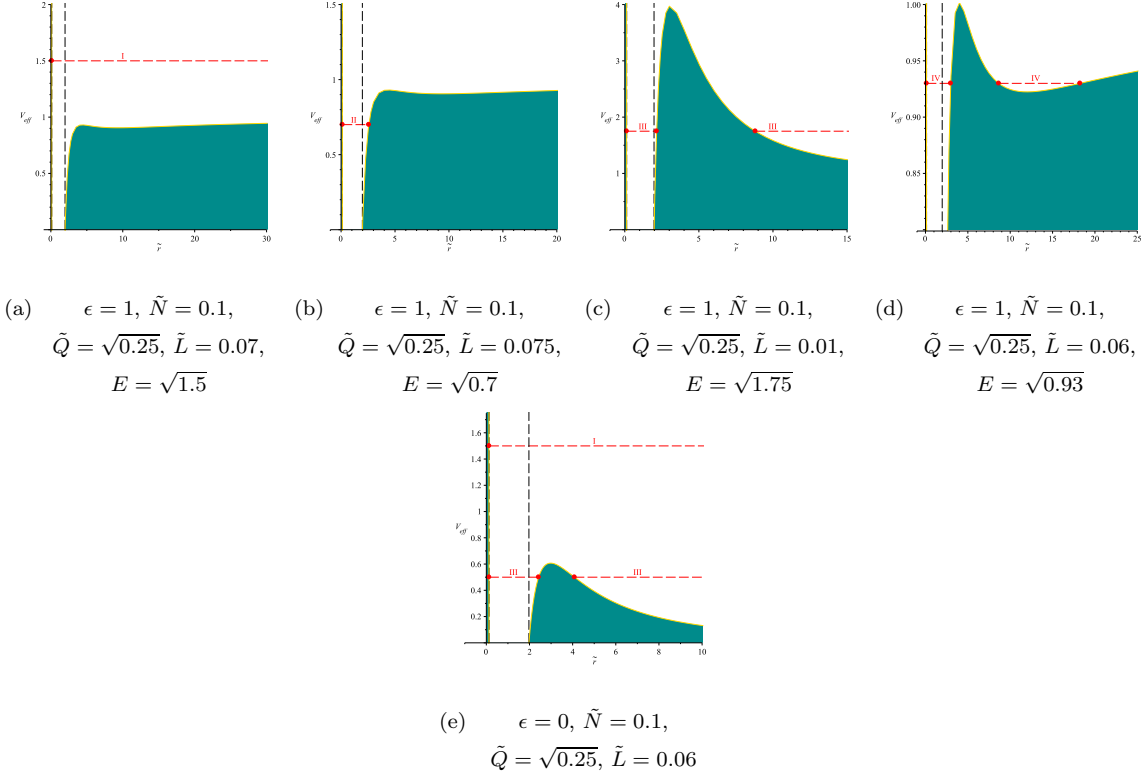


FIG. 10: Plots of the effective potential for the different orbit types of Table V, for the case of phantom surrounding field with the parameters $k\lambda = 4$. The horizontal red-dashed lines denotes the squared energy parameter E^2 . The vertical black dashed lines show the position of the horizons. The red dots marks denote the zeros of the polynomial R , which are the turning points of the orbits. In the cyan area, no motion is possible since $\tilde{R} < 0$.

region	pos.zeros	range of \tilde{r}	orbit
I	1		TEO
II	2		MBO
III	3		MBO, EO
IV	4		MBO, BO

TABLE V: Types of orbits of the phantom surrounding field. The range of the orbits is represented by thick lines. The dots show the turning points of the orbits. The positions of the two horizons are marked by a vertical double line. The single vertical line indicates the singularity at $\tilde{r} = 0$.

In all surrounding fields (quintessence, dust, radiation, cosmological constant and phantom fields), when Rastall geometric parameter becomes zero, the results are reduce to a Reissner-Nordström black hole (see Fig. 11 (a) and table VI) and when both electric charge and Rastall geometric parameter become zero, the metric and results are same as a Schwarzschild black hole (see Fig. 11 (b) and table VII) as our expectation. In addition the possible types of orbits for a Reissner-Nordström black hole are BO, EO, TEO and MBO while for a Schwarzschild black hole are TO, EO and BO. However by comparing between table VII and tables of all other cases (I-VI), we can be seen that terminating orbit (TO) has appeared, in which test particles come from certain point and fall into singularity of a Schwarzschild black hole, while this orbit cannot appear for all other discussed cases included electrical charged.

region	pos.zeros	range of \tilde{r}	orbit
I	1		TEO
II	2		MBO
III	3		MBO, EO
IV	4		MBO, BO

TABLE VI: Types of orbits of a Reissner-Nordström black hole. The range of the orbits is represented by thick lines. The dots show the turning points of the orbits. The positions of the two horizons are marked by a vertical double line. The single vertical line indicates the singularity at $\tilde{r} = 0$.

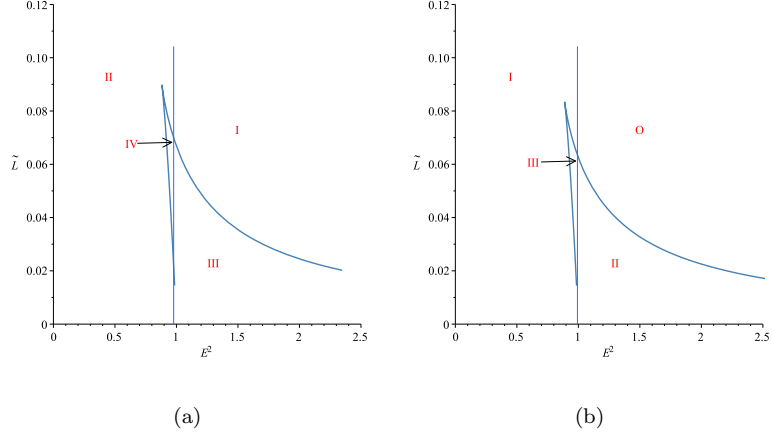


FIG. 11: Plots of $L - E^2$ diagram and region of different types of geodesic motion (a): Reissner-Nordström ($N = 0$) and (b): Schwarzschild ($N = Q = 0$) geodesics. The numbers of positive real zeros in these regions are: O=0, I=1, II=2, III=3, IV=4.

region	pos.zeros	range of \tilde{r}	orbit
O	0		TO
I	1		TO
II	2		TO, EO
III	3		TO, BO

TABLE VII: Types of orbits of a Schwarzschild black hole. The range of the orbits is represented by thick lines. The dots show the turning points of the orbits. The positions of the horizon is marked by a vertical double line. The single vertical line indicates the singularity at $\tilde{r} = 0$.

4.1. Examples of trajectory of particle motion and light

In this section, we show some possible orbits for discussed space-times in previous sections.

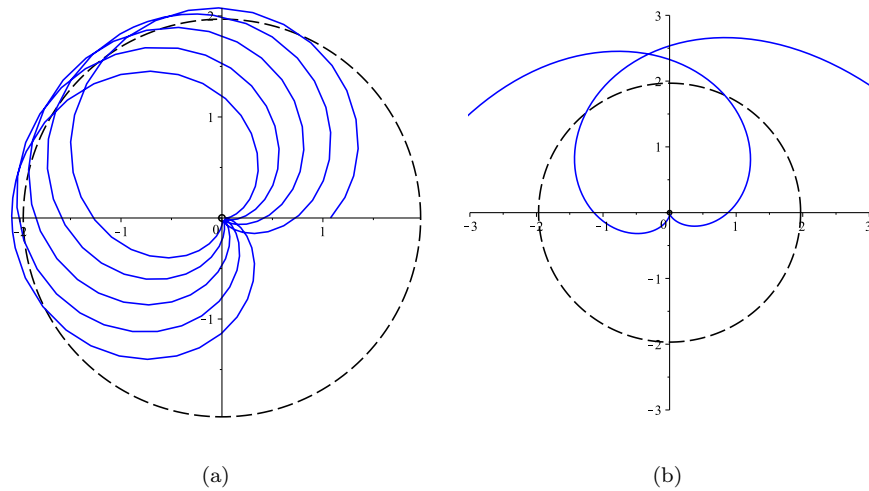


FIG. 12: Possible orbits for the quintessence surrounding field for $k\lambda = \frac{1}{4}$ corresponding to the table I. (a): Many-world Bound Orbit, with parameters $\tilde{Q} = 0.45$, $E = \sqrt{0.93}$ and (b): Two-world Escape Orbit with parameters $\tilde{Q} = \sqrt{0.25}$, $E = \sqrt{0.93}$, $\tilde{N} = 0.12$, $L = 0.06$. The blue lines show the path of the orbits and the circles represent two horizons.

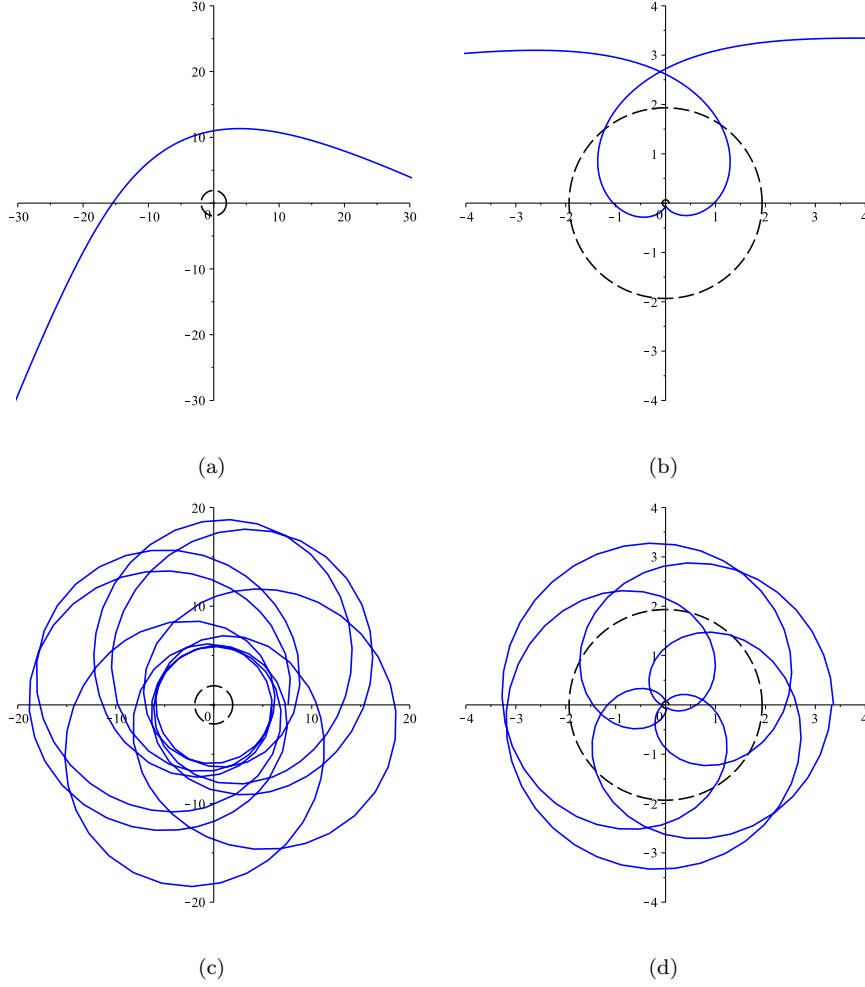


FIG. 13: Possible orbits for a black hole surrounded by radiation field corresponding to table IV. (a): Escape Orbit, with parameters $\tilde{Q} = 0.45$, $E = \sqrt{0.93}$, (b): Two-world Escape Orbit with parameters $\tilde{Q} = \sqrt{0.25}$, $E = \sqrt{0.93}$, $\tilde{N} = 0.12$, $L = 0.06$, (c): Bound Orbit, with parameters $\tilde{Q} = 0.45$, $E = \sqrt{0.93}$ and (d): Many-world Bound Orbit with parameters $E = \sqrt{0.93}$, $\tilde{N} = 0.12$ and $\tilde{Q} = \sqrt{0.25}$. The blue lines show the path of the orbits and the circles represent two horizons.

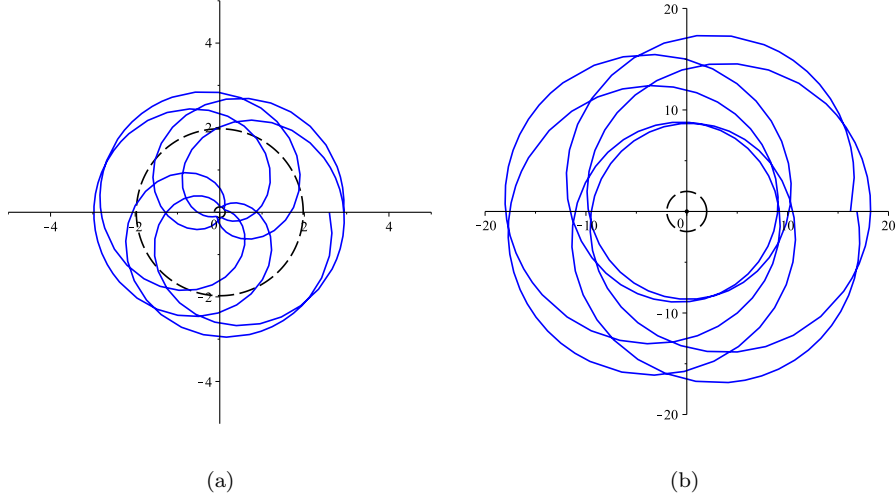


FIG. 14: Possible orbits for the phantom surrounding field for $k\lambda = \frac{2}{3}$ corresponding to table V. (a): Many-world Bound Orbit, with parameters $\tilde{Q} = 0.45$, $E = \sqrt{0.93}$ and (b): Bound Orbit with parameters $E = \sqrt{0.93}$, $L = 0.06$, $\tilde{N} = 0.12$. The blue lines show the path of the orbits and the circles represent two horizons.

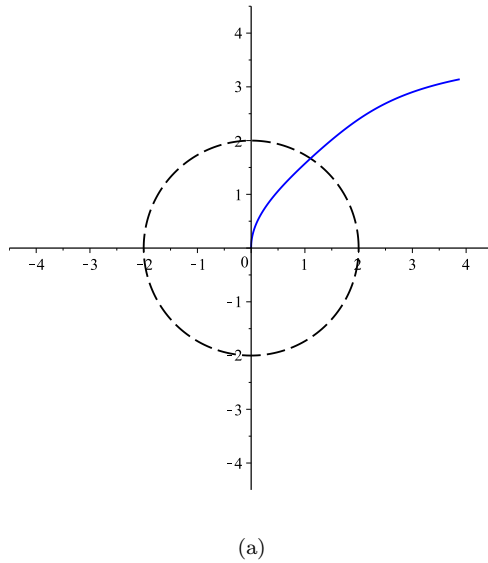


FIG. 15: Terminating orbits for a Schwarzschild black hole corresponding to table VII with parameters $E = \sqrt{0.93}$, $L = 0.06$, $\tilde{N} = 0$ and $\tilde{Q} = 0$. The blue line shows the path of the orbit and the circle represents the horizon.

5. CONCLUSIONS

In this paper, the analytical solution of geodesic motion for massless and massive test particles in the vicinity of a black hole space-time surrounded by perfect fluid in the context of Rastall gravity has been presented. We have studied the timelike and null geodesics equations of motion for the black hole surrounded by cases quintessence, dust, radiation, cosmological constant and phantom fields in detail. In each case, we obtain the analytical solutions by regarding and constraint on effective state parameter ω_{eff} and considering some possible values of Rastall coupling constant $k\lambda$, so that equation of motion included integer powers of r and also can be solved analytically.

For a black hole surrounded by quintessence field with $\omega_q = -\frac{2}{3}$, two possible cases of $k\lambda$ ($k\lambda = \frac{1}{4}$, $k\lambda = -2$) analysed. For the case $k\lambda = -2$, the equation of motion have included the term $\frac{N_q}{r}$ as Rastalls correction term in which here the field structure parameter N_q can play the role of the mass of black hole, but with the case $k\lambda = \frac{1}{4}$, the term $N_q r^2$ has appeared in which the filed structure parameters N_q , can describe the acceleration of the Universe. When dust field has considered as a background fluid with $\omega_d = 0$, also two possible cases of $k\lambda$ ($k\lambda = \frac{2}{9}$, $k\lambda = \frac{1}{4}$) has been analysed, in which for the case $k\lambda = \frac{2}{9}$, the equation of motion has contained Rastall correction term $N_d r$, in which here Rastall geometric parameter N_d , can play the role of small and large-scale physical evidence for the ranges of scalar curvature [45], and for the case $k\lambda = \frac{1}{4}$, the Rastalls correction term $N_d r^2$ has appeared in which field structure constant N_d , similar to the same case in quintessence filed, play the role of accelerating expansion of the Universe. When radiation is considered as a background field with $\omega_r = \frac{1}{3}$, the metric is Reissner-Nordström metric of a black hole, which the field structure parameter N_r with the electric charge Q , behave role of the effective charge of this black hole ($\sqrt{Q^2 - N_r}$). When we consider a black hole is surrounded by cosmological constant field with $\omega_c = -1$, the metric is same as Kieslev metric in GR which was achieved previously. Therefore the term $N_c r^2$ as Rastall correction term will appear, in which the Rastall geometric parameter N_c causes the role of accelerating expansion of the Universe, same as quintessence and also dust field.

Finally for a black hole surrounded by the phantom field with $\omega_p = -\frac{4}{3}$, three cases of $k\lambda$ ($k\lambda = \frac{1}{4}$, $k\lambda = \frac{2}{3}$, $k\lambda = 4$) are possible values which have been analysed. For two cases ($k\lambda = \frac{1}{4}$, $k\lambda = \frac{2}{3}$), Rastall correction term has appeared in terms of $N_p r$ and $N_p r^2$, which

in the term $N_p r$, Rastall geometric parameter N_p can play the role of small and large-scale physical evidence for the ranges of scalar curvature [45] and in the term $N_p r^2$, field structure parameter N_p play the role of accelerating expansion of the Universe, but for the case $k\lambda = 4$, field structure parameter N_p behaves mass role i.e. $\frac{1}{r}$ same as the quintessence field. After reviewing the space-time and the corresponding equations of motion, we classified the complete set of orbit types for massive and massless test particles moving on geodesics for each case. In addition, it has shown in table VI when Rastall geometric parameter vanish, the metrics reduce to Reissner-Nordström black holes, while it has shown in table VII when the electric charge of a black hole becomes zero the results decrease to Schwarzschild. The geodesic equations solved analytically by Weierstrass elliptic and derivatives of hyperelliptic Kleinian sigma functions. We also considered all possible types of orbits. Using effective potential techniques and parametric diagrams, the possible types of orbits were derived. For null geodesics EO, TEO and MBO are possible, while for timelike geodesics EO, TEO, BO and MBO are possible. Examples of such possible types of orbits were shown in the Sec. 4.1.

-
- [1] E. Hackmann and C. Lammerzahl, “Geodesic equation in Schwarzschild- (anti-) de Sitter space-times: Analytical solutions and applications,” *Phys. Rev. D* **78**, 024035 (2008) doi:10.1103/PhysRevD.78.024035 [arXiv:1505.07973 [gr-qc]].
 - [2] C. Lammerzahl, Testing Basic Laws of Gravitation Are Our Postulates on Dynamics and Gravitation Supported by Experimental Evidence?, *Fundamental Theories of Physics* **162**, DOI 10.1007/978-90-481-3015-3 2,
 - [3] S. Soroushfar, R. Saffari and A. Jafari, “Study of geodesic motion in a (2+1)-dimensional charged BTZ black hole,” *Phys. Rev. D* **93**, no. 10, 104037 (2016) doi:10.1103/PhysRevD.93.104037 [arXiv:1512.08449 [gr-qc]].
 - [4] D. Clowe et al, *Astrophys. J.* **648**, L109 (2006).
 - [5] J. F. Navarro, C. S. Frenk, S. D.M. White, *Astrophys. J.* **490**, 493 (1997).
 - [6] A.G. Riess et al. Observational Evidence from Supernovae for an Accelerating Universe and a Cosmological Constant. *Astronom. J.*, **116**:1009, (1998). S. Perlmutter et al. Measurements of omega and lambda from 42 high-redshift supernovae. *Astrophys. J.*, **517**:565, (1999).

- [7] A. G. Riess et al., *Astrophys. J.* **560**, 49 (2001).
- [8] Joshua A. Frieman,^{1,2} Michael S. Turner,² and Dragan Huterer, *Annu. Rev. Astron. Astrophys.*, **46**:385432 (2008).
- [9] S. Fernando, “Schwarzschild black hole surrounded by quintessence: Null geodesics,” *Gen. Rel. Grav.* **44**, 1857 (2012) doi:10.1007/s10714-012-1368-x [arXiv:1202.1502 [gr-qc]].
- [10] I. Radinschi, T. Grammenos and A. Spanou, “Distribution of Energy-Momentum in a Schwarzschild-Quintessence Space-time Geometry,” *Int. J. Theor. Phys.* **52**, 4100 (2013) doi:10.1007/s10773-013-1724-y [arXiv:1204.1663 [gr-qc]].
- [11] D. N. Spergel et.al. (WMAP Collaboration), *Wilkinson Microwave Anisotropy Probe (WMAP) Three Year Results: Implications for Cosmology*, *Astrophys.J.Suppl.***170** 377 (2007)
- [12] M. Tegmark, et al., *Cosmological parameters from SDSS and WMAP* , *Phys. Rev. D* **69** 103501 (2004), [arXiv:astro-ph/0310723v2]. M. Colless, et al., *The 2dF Galaxy Redshift Survey: Spectra and redshifts* , *Mon. Not. R. Astron. Soc.* **328** 1039 (2001), [arXiv:astro-ph/0106498v3]. S. Cole, et al., *The 2dF Galaxy Redshift Survey:Power-spectrum analysis of the final dataset and cosmological implications*, *Mon. Not. R. Astron. Soc.* **362** 505 (2005), [arXiv:astro-ph/0501174v2]. V. Springel, C. S. Frenk, and S. M. D. White, *The large-scale structure of the Universe*, *Nature(London)*. **440** 1137 (2006), [arXiv:astro-ph/0604561].
- [13] J. L. Tonry et al. [Supernova Search Team Collaboration], *Astrophys. J.* **594**, 1 (2003) [astro-ph/0305008]. A. G. Riess et al., *Astrophys.J.* **607**, 665 (2004). P. deBernardis, et al., *A flat Universe from high-resolution maps of the cosmic micro wave background radiation*, *Nature* **404** 955 (2000), [arXiv:astro-ph/0004404v1].
- [14] V. Sahni, A. Krasinski and Ya.B. Zeldovich, *Republication of: The cosmological constant and the theory of elementary particles (By Ya. B. Zeldovich)*. *Gen. Rel. Grav.* **40**, 1557-1591 (2008), *Sov. Phys. Usp.* **11** 381-393 (1968).
- [15] Zhaoyi Xu, Jiancheng Wang, *Kerr-Newman-AdS Black Hole Surrounded By Scalar Field Matter In Rastall Gravity*, arXiv:1711.04542v1 [gr-qc] 13 Nov 2017. Zhaoyi Xu, Jiancheng Wang, *Kerr-Newman-AdS Black Hole In Quintessential Dark Energy*, arXiv:1609.02045v3 [gr-qc] 10 Mar 2017.
- [16] S. Weinberg, *The Cosmological Constant Problem*. *Rev. Mod. Phys.* **61**, 1-23 (1989); S. M. Carroll, *The Cosmological Constant*. *Living Rev.Rel.* **4**:1,2001 [astro-ph/0004075]; T. Padmanabhan, *Cosmological Constant: The Weight Of The Vacuum*. *Phys. Rept.* **380**, 235-320

- (2003).
- [17] S. Fernando, *Mod. Phys. Lett. A* **28**, 1350189 (2013) doi:10.1142/S0217732313501897 [arXiv:FERNANDO:2013uxa.5064 [gr-qc]].
- [18] V. V. Kieslev, Quintessence and black holes, *Class. Quantum Grav.* **20** 11871197 (2003).
- [19] Y. Heydarzade and F. Darabi, “Black Hole Solutions Surrounded by Perfect Fluid in Rastall Theory,” *Phys. Lett. B* **771**, 365 (2017) doi:10.1016/j.physletb.2017.05.064 [arXiv:1702.07766 [gr-qc]].
- [20] G.W. Gibbons, S.W. Hawking, *Phys. Rev. D* **15** (1977) 2738. L. Parker, *Phys. Rev. D* **3** (1971) 346; L. Parker, *Phys. Rev. D* **3** (1971) 2546. L.H. Ford, *Phys. Rev. D* **35** (1987) 2955. C.E.M. Batista, M.H. Daouda, J.C. Fabris, O.F. Piattella, D.C. Rodrigues, *Phys. Rev. D* **85** (2012) 084008. S.H. Pereira, C.H.G. Bessa, J.A.S. Lima, *Phys. Lett. B* **690** (2010) 103. S. Calogero, *J. Cosmol. Astropart. Phys.* **11** (2011) 016. S. Calogero, H. Velten, *J. Cosmol. Astropart. Phys.* **11** (2013) 025. H. Velten, S. Calogero, arXiv:1407.4306.
- [21] N. D. Birrell, P. C. W. Davies, *Quantum fields in Curved Space*, (Cambridge University Press, Cambridge, 1982).
- [22] Rastall P (1972) Generalization of the einstein theory. *Physical Review D* **6**:3357. , P. Rastall, *Can. J. Phys.* 54 (1976) 66.
- [23] H. Moradpour, Thermodynamics of flat FLRW universe in Rastall theory, *Physics Letters B* **757** (2016) 187191. arXiv:1601.04529v6 [physics.gen-ph] 24 Dec 2016.
- [24] V. Majernik and L. Richterek, “Rastall’s gravity equations and Mach’s principle,” gr-qc/0610070.
- [25] T. Carams, J. C. Fabris, O. F. Piattella, V. Stokov, M. H. Daouda and A. M. Oliveira, arXiv:1503.04882 [gr-qc].
- [26] Y. Heydarzade, H. Moradpour and F. Darabi, *Can. J. Phys.* **95**, no. 12, 1253 (2017) doi:10.1139/cjp-2017-0254 [arXiv:1610.03881 [gr-qc]].
- [27] A. M. Oliveira, H. E. S. Velten, J. C. Fabris and L. Casarini, *Phys. Rev. D* **92**, no. 4, 044020 (2015) doi:10.1103/PhysRevD.92.044020 [arXiv:1506.00567 [gr-qc]].
- [28] H. Moradpour, N. Sadeghnezhad and S. H. Hendi, *Can. J. Phys.* **95**, no. 12, 1257 (2017) doi:10.1139/cjp-2017-0040 [arXiv:1606.00846 [gr-qc]].
- [29] H. Moradpour and I. G. Salako, *Adv. High Energy Phys.* **2016**, 3492796 (2016) doi:10.1155/2016/3492796 [arXiv:1606.06589 [gr-qc]].

- [30] A. M. Oliveira, H. E. S. Velten and J. C. Fabris, *Phys. Rev. D* **93**, no. 12, 124020 (2016) doi:10.1103/PhysRevD.93.124020 [arXiv:1602.08513 [gr-qc]].
- [31] K. A. Bronnikov, J. C. Fabris, O. F. Piattella and E. C. Santos, *Gen. Rel. Grav.* **48**, no. 12, 162 (2016) doi:10.1007/s10714-016-2152-0 [arXiv:1606.06242 [gr-qc]].
- [32] H. Moradpour, Y. Heydarzade, F. Darabi and I. G. Salako, *Eur. Phys. J. C* **77**, no. 4, 259 (2017) doi:10.1140/epjc/s10052-017-4811-z [arXiv:1704.02458 [gr-qc]].
- [33] N.D. Birrell, P.C.W. Davies, *Quantum Fields in Curved Space*, (Cambridge University Press, Cambridge, 1982).
- [34] R. Bertlmann, *Anomalies in Quantum Field Theory*, Oxford University Press, Oxford, 2000.
- [35] T. S. Almeida, M. L. Pucheu, C. Romero and J. B. Formiga, *Phys. Rev. D* **89**, no. 6, 064047 (2014) doi:10.1103/PhysRevD.89.064047 [arXiv:1311.5459 [gr-qc]].
- [36] E. Hackmann, arXiv:1506.00804 [gr-qc].
- [37] S. Soroushfar, R. Saffari and E. Sahami, “Geodesic equations in the static and rotating dilaton black holes: Analytical solutions and applications,” *Phys. Rev. D* **94**, no. 2, 024010 (2016) doi:10.1103/PhysRevD.94.024010 [arXiv:1601.03143 [gr-qc]].
- [38] K. Schwarzschild, *Sitzungsber. Preuss. Akad. Wiss. Berlin (Math. Phys.)*, **424** (1916) [physics/9912033].
- [39] Y. Hagihara, *Jpn. J. Astron. Geophys.* **8**, 67 (1931).
- [40] E. Hackmann, V. Kagramanova, J. Kunz and C. Lammerzahl, *Phys. Rev. D* **78**, 124018 (2008) Erratum: [*Phys. Rev.* **79**, 029901 (2009)] Addendum: [*Phys. Rev. D* **79**, no. 2, 029901 (2009)] doi:10.1103/Phys.Rev.D. **79**.029901, 10.1103/Phys.Rev.D. **78**.124018, 10.1103/Phys.Rev. **79**.029901 [arXiv:0812.2428 [gr-qc]].
- [41] S. Chandrasekhar, *The mathematical theory of black holes*, (Clarendon press, Oxford, 1985).
- [42] E. Hackmann and C. Lammerzahl, “Complete Analytic Solution of the Geodesic Equation in Schwarzschild- (Anti-) de Sitter space-times,” *Phys. Rev. Lett.* **100**, 171101 (2008) doi:10.1103/PhysRevLett.100.171101 [arXiv:1505.07955 [gr-qc]].
- [43] R. P. Kerr, *Phys. Rev. Lett.* **11**, 237 (1963).
- [44] E. Hackmann, C. Lammerzahl, V. Kagramanova and J. Kunz, *Phys. Rev. D* **81**, 044020 (2010) [arXiv:1009.6117 [gr-qc]].
- [45] S. Soroushfar, R. Saffari, J. Kunz and C. Lmmerzahl, “Analytical solutions of the geodesic equation in the space-time of a black hole in f(R) gravity,” *Phys. Rev. D* **92**, no. 4, 044010

- (2015) doi:10.1103/PhysRevD92.044010 [arXiv:1504.07854 [gr-qc]].
- [46] B. Hoseini, R. Saffari, S. Soroushfar, J. Kunz and S. Grunau, “Analytic treatment of complete geodesics in a static cylindrically symmetric conformal space-time,” *Phys. Rev. D* **94**, no. 4, 044021 (2016) doi:10.1103/PhysRevD.94.044021 [arXiv:1602.03898 [gr-qc]].
- [47] V. Z. Enolski, E. Hackmann, V. Kagramanova, J. Kunz and C. Lammerzahl, *J. Geom. Phys.* **61**, 899 (2011) [arXiv:1011.6459 [gr-qc]].
- [48] V. Kagramanova and S. Reimers, *Phys. Rev. D* **86**, 084029 (2012); V. Diemer, J. Kunz, C. Lämmerzahl and S. Reimers, *Phys. Rev. D* **89**, no. 12, 124026 (2014)
- [49] S. Soroushfar, R. Saffari, S. Kazempour, S. Grunau and J. Kunz, “Detailed study of geodesics in the Kerr-Newman-(A)dS space-time and the rotating charged black hole space-time in $f(R)$ gravity,” *Phys. Rev. D* **94**, no. 2, 024052 (2016) doi:10.1103/PhysRevD.94.024052 [arXiv:1605.08976 [gr-qc]].
- [50] V. V. Kieslev, *Class Quantum Gravity* **20** (2003), 1187.
- [51] B. Hartmann and P. Sirimachan, *JHEP* **1008**, 110 (2010) [arXiv:1007.0863 [gr-qc]].
- [52] E. Hackmann and C. Lammerzahl, *AIP Conf. Proc.* **1577**, 78 (2014) doi:10.1063/1.4861945 [arXiv:1506.00807 [gr-qc]].
- [53] V. M. Buchstaber, V. Z. Enolskii, and D. V. Leykin, (Gordon and Breach, New York, 1997).